

Comparisons Between Observed and Simulated Ice Motion in the Northern Baltic Sea

Zhanhai Zhang

Department of Geophysics, University of Helsinki, Finland¹

Abstract

Sea ice drift in the coastal ice zone of the Bothnian Bay was measured with five GPS drifters in March 1997. To model coastal ice dynamics, the viscous-plastic ice model of Hibler with a fine spatial resolution of 5 km is used. A truncated elliptical yield curve is used preventing any tensile stress from occurring. Thermodynamics are neglected because our interest is in ice dynamics. The model simulation is run for 20 days, which covers the whole experiment period. The results show that the observed characteristics of the pack ice motion can be realistically simulated by the model. The ice drift trajectories obtained from the model demonstrate good agreement with drifter data in most of the period. Comparison of modeled ice displacements with sequential SAR data on the basin wide scale is also made and the agreement is in general quite good. The ice field in the coastal ice zone illustrated strong rigid and plastic patterns, suggesting an ice strength constant $P^=3.0 \times 10^4 \text{ N/m}^2$ being best representative.*

Key words: Sea ice model, ice dynamics, ice drift, Baltic Sea

1. Introduction

Sea ice motion is mainly wind driven in the Baltic Sea. Solid boundary (coastline or fast ice boundary) highly influences the ice motion and thickness redistribution. The internal ice stress, depending on the ice conditions and the boundary geometry, is an important factor and has the same order of magnitude as the wind stress for high ice concentrations and strengths. An early study of *Leppäranta* (1981) indicated that the solid boundary results in heavy ice deformation in the Bay of Bothnia. The solid boundary, on the other hand, causes open water formation when the ice moves away from it. Therefore, large spatial and temporal variations in ice velocity and thickness redistribution occur through the generation of leads and deformed ice.

¹present address: National Research Center for Marine Environment Forecast, No. 8 Da Hui Si, Haidian Division 100081 Beijing, China

Dynamics of the sea ice cover is an important process to consider in the ice modeling. Ice model existed can be divided into two categories: discrete model (e.g., *Hopkins*, 1996) and continuum model (e.g., *Hibler*, 1979). The continuum model due to its simplicity has been widely used in different model grid scales from 100 km in the Arctic Ocean to 10 km in the seasonal ice zone (e.g., *Wu and Leppäranta*, 1990; *Leppäranta and Zhang*, 1992). However, the use of the continuum model is restricted so that it must satisfy such a condition that the ice motion of individual floes and leads is neglected, *i.e.*, the system must include sufficient ice floes so that it can be treated as a continuum medium. Thus, the model grid size depends on the mean ice floe size.

A sea ice experiment ZIP-97 (Zooming of Ice Physics, 1997), a part of a project “Local Ice Cover Deformation and Mesoscale Ice Dynamics” (ICE STATE), has been carried out in the Baltic Sea in March 1997 (*Haapala and Leppäranta*, 1997). ZIP-97 offered the first opportunity to study sea ice drift and deformation with a GPS drifter array in the Baltic Sea. The drifter data is an important part of the ZIP-97 being a link between the basin scale ice dynamics and the local scale deformations; one of the main objectives of the ICE STATE project is to study connections between different scales in ice dynamics. Five drifters were deployed in the Bay of Bothnia on 10–20 kilometers spatial scale.

A dynamic sea ice model is used to simulate the ice dynamics in the ZIP-97 case. The model is based on *Hibler* (1979) viscous-plastic ice model. However, many new features have been added. In addition to the elliptical yield curve, a more realistic truncated elliptical yield curve is chosen. An efficient numerical method for solving momentum balance proposed by *Zhang and Hibler* (1997) is used instead of the old procedure of *Hibler* (1979), and a moving ice/water boundary has been taken into account. To realistically simulate ice motion near the coasts, a no-slip/free boundary condition is used. The present paper shows model results and comparisons with observed data. One goal is to examine how well a continuum model can reproduce the ice motion on the fine scale of 5 km.

2. Model description

The present model is based on *Hibler's* (1979) viscous-plastic ice model. The momentum balance equation involves the inertial term, Coriolis force, air stress, water stress and internal ice stress. The ice mass conservation is described by two-level ice thickness distribution equations. Thermodynamics are not included because our interests are the dynamic process of sea ice. This is a good approximation for the first half of the ZIP-97 period but may slightly underestimate the rigidity of the ice in the latter half. The air and water stresses are parameterized by the well-known quadratic drag laws. The air drag coefficient is 1.8×10^{-3} (*Haapala and Leppäranta*, 1996) and the turning angle is zero because the surface wind is used. The ocean current field beneath the frictional surface layer is assumed equal to zero, and the corresponding ice/water drag co-

efficient is $C_w = 3.5 \times 10^{-3}$ and turning angle $\theta = 18^\circ$ (Leppäranta and Omstedt, 1990). Again this is a source of some inaccuracy; but anyway the main forces in the ice dynamics were the wind stress and internal friction of ice in the study case. The internal ice stress tensor is obtained using the nonlinear viscous-plastic constitutive rheology of Hibler (1979)

$$\boldsymbol{\sigma} = 2\eta\dot{\boldsymbol{\varepsilon}} + (\zeta - \eta)\text{tr}\dot{\boldsymbol{\varepsilon}}\mathbf{I} - P\mathbf{I} / 2 \quad (1)$$

$$\zeta = P / 2\Delta, \quad \eta = \zeta / e^2, \quad (2a,b)$$

$$\Delta = [(\dot{\varepsilon}_1 + \dot{\varepsilon}_2)^2 + (\dot{\varepsilon}_1 - \dot{\varepsilon}_2)^2 / e^2]^{1/2} \quad (3)$$

where $\dot{\boldsymbol{\varepsilon}}$ is strain rate tensor, \mathbf{I} is the unit tensor, ζ and η are nonlinear bulk and shear viscosities, e is the aspect ratio of the yield curve, $\dot{\varepsilon}_1$ and $\dot{\varepsilon}_2$ are the principal strain rates, and P is the ice strength expressed by

$$P = P^* h \exp(-C(1 - A)) \quad (4)$$

where P^* is the ice strength constant and C is the strength reduction constant for opening, h is mean ice thickness and A is ice compactness.

To avoid occurrence of arbitrarily large of ζ and η for very small strain rates, Δ is bounded below by the maximum viscous creep $\dot{\varepsilon}_0$ that describes how easily the stress state can reach the yield curve. When $\Delta > \dot{\varepsilon}_0$, the ice moves as a plastic fluid, otherwise it moves as a linear viscous fluid. To well approximate the plastic behavior, the creep limit $\dot{\varepsilon}_0$ has to be small enough. In the present simulation, we set $\dot{\varepsilon}_0 = 10^{-10} \text{ s}^{-1}$ which is less by 2–3 order of magnitude than the measurement accuracy.

The yield curve described by equation (1) is an ellipse in the principal stress space, and its size and shape are specified by P and e . However, the use of this yield curve and normal flow rule leads to unphysical effects (tensile strength >0) whenever the stress state lies in the fourth (or the second) quadrant. To avoid this, we follow the idea described by Hibler and Schulson (1997) to prevent any tensile stress from occurring in such a way that the first principal stress value σ_1 is limited by zero, $\sigma_2 \leq \sigma_1 \leq 0$, where σ_1 and σ_2 are the principal stress components of the stress tensor $\boldsymbol{\sigma}$

$$\sigma_{1,2} = \zeta(\dot{\varepsilon}_1 + \dot{\varepsilon}_2) \pm \eta(\dot{\varepsilon}_1 - \dot{\varepsilon}_2) - P / 2 \quad (5a,b)$$

If we define η such that

$$\eta = \frac{P / 2 - \zeta(\dot{\varepsilon}_1 + \dot{\varepsilon}_2)}{|\dot{\varepsilon}_1 - \dot{\varepsilon}_2|} \quad (6)$$

then the condition $\sigma_1 \leq 0$ will always be satisfied.

Thus the yield curve in the present model is an elliptical truncated yield curve as seen in Fig. 1. It describes a rheology with no tensile stress and the shear stress under divergent conditions is substantially reduced compared with the conventional elliptical yield curve.

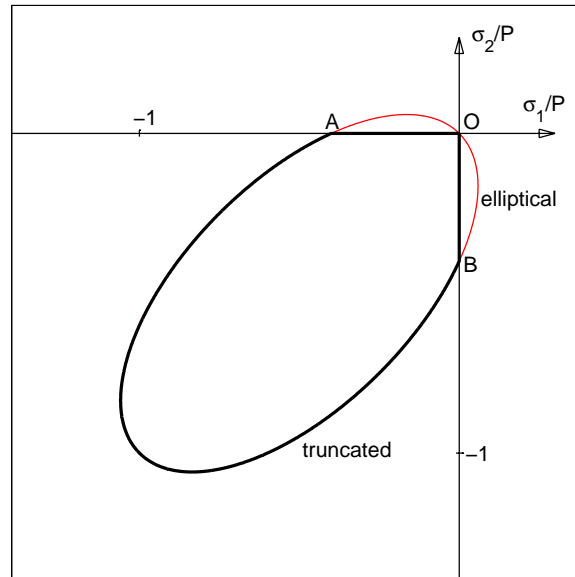


Fig. 1. Elliptical yield curves in normalized principal stress space (σ_1 and σ_2 are the principal stresses). Bold curve OABO defines the elliptical truncated yield curve.

To simulate the GPS drifter trajectories, the model grid size should be able to distinguish between different drifters. In the present case the grid size is 5 km, half of the size normally used in the Baltic Sea (*Haapala and Leppäranta, 1996*). We expect that this grid size does not severely violate the continuum approximation in the Hibler model, it is, in fact, still one order of magnitude larger than typical ice floe size (*Leppäranta, 1981*). The time step is 15 minutes. The model boundaries consist of both solid boundary and lateral ice/water moving boundary. Because the drifter locations in our case were very close to the land fast ice boundary, formulation of the boundary condition on the solid boundary is crucial in the simulation. On the solid boundary a no-slip/free boundary condition is proposed, i.e., the ice velocity is set to zero when ice moves toward the boundary, otherwise it is equal to the mean value of adjacent internal points. An analogous treatment is adopted for the lateral ice/water boundary. The ice velocity is set equal to the mean value of adjacent internal points when the velocity is directed toward interior, otherwise it is equal to the free-drift velocity. Thus, the lateral ice/water boundary is assumed to be of a stress-free type.

3. Results

3.1 Weather and ice conditions

The weather and ice conditions during the experiment period are shown in Figs 2–3. We see that the weather conditions can be divided into two periods. In the first period (3–13 March) the weather was warm and the air temperature was around 0°C. Southwesterly and westerly winds prevailed with strong wind events on 5, 9 and 13 March. The thickness distribution of the ice illustrated a large variability in time and space due to the wind forcing. The level ice thickness on 3 March was typically 30–50 cm in the eastern part of the bay and decreased westward to 10–30 cm near the ice edge. There were heavy ridged and rafted areas along the eastern fast ice edge. In the next five days the ice field was further compacted and the ice cover area decreased due to the strong winds. In the second period, after 14 March, cold northerly winds dominated and the air temperature consequently dropped down between -5° to -15°C. The ice cover was driven southwestward by the wind, forming open leads in the northern part of the bay. A large area of pack ice was separated from the heavily consolidated ice zone in the eastern part (see the ice map 20.3 in Fig. 3b). As the ice dispersed, the sea surface was exposed to the air. The thermal heat budget and the force balance were changed and new ice formed in the north. The Bay of Bothnia was again totally ice covered around 24 March.

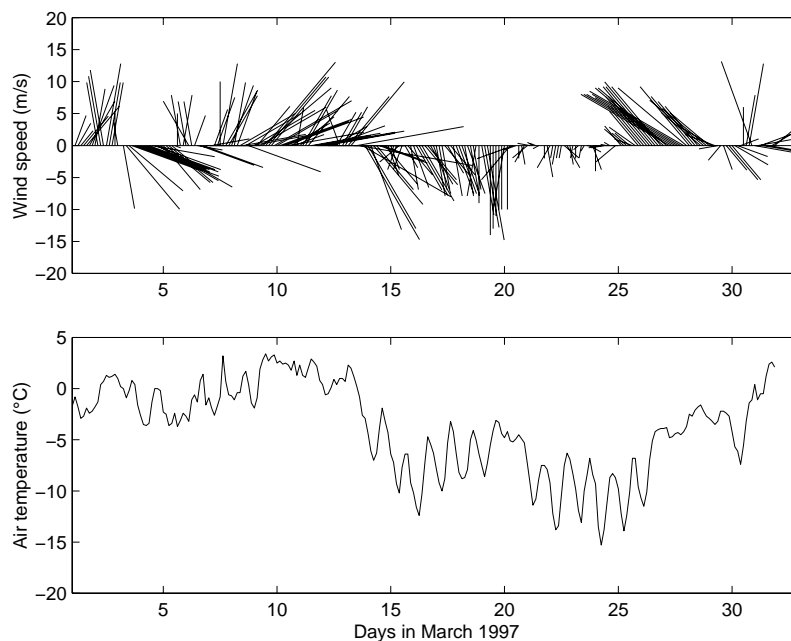


Fig. 2. Wind and air temperature in March 1997 at Kemi-1 station (24°06'E, 65°23'N, 26 meters above sea level).

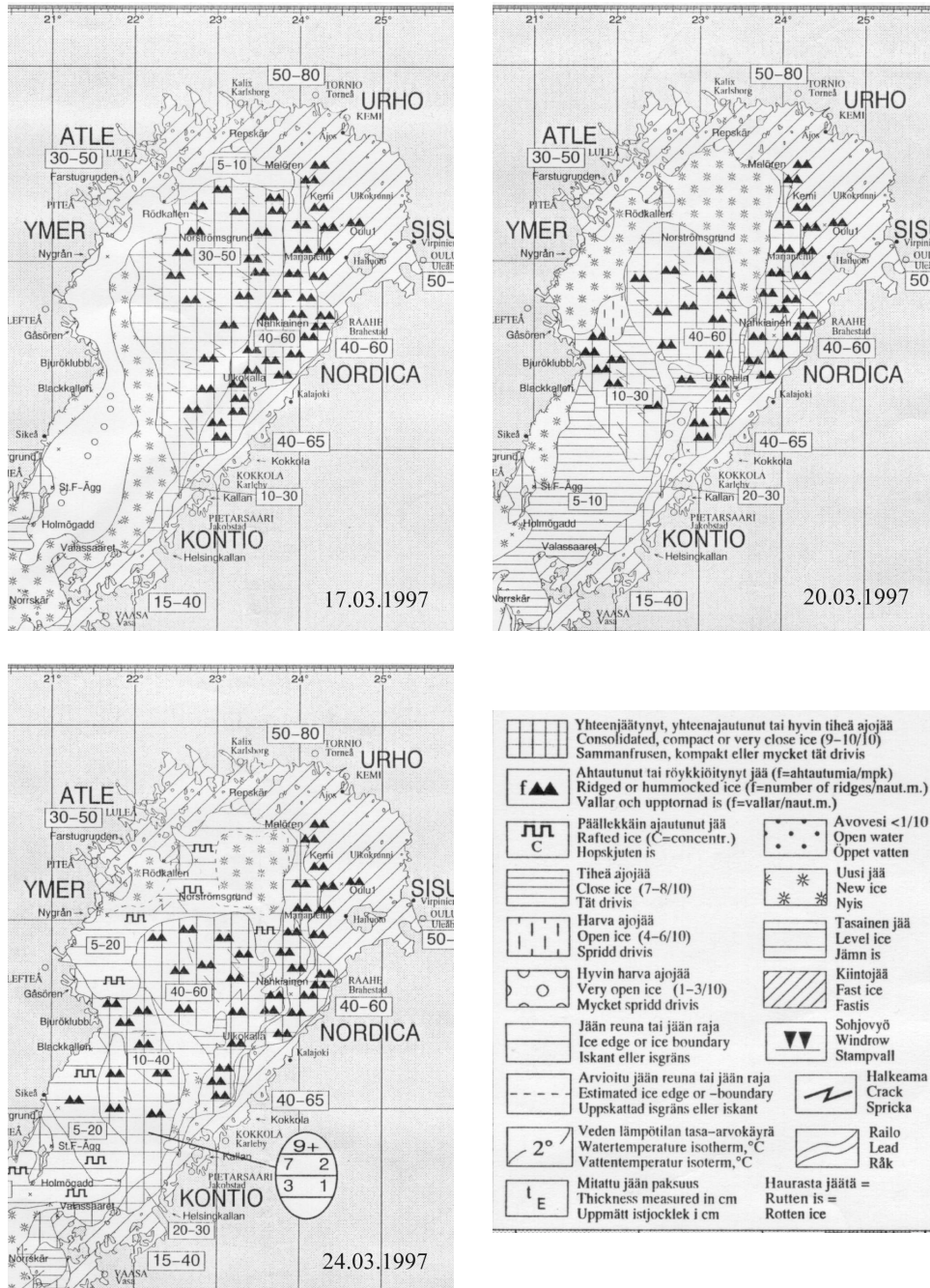


Fig. 3b. Observed ice conditions from 17 to 24 March 1997.

3.2 Initial condition, wind forcing data and model parameters

The input of the model consists of ice thickness, ice compactness and wind stress. The initial ice thickness and compactness were obtained from the Finnish Institute of Marine Research (FIMR) ice chart of 3 March. The typical level ice thickness was 30–50 cm in the eastern part and 10–30 cm in the west and south parts. The compactness was more than 90% over most of the ice-covered area. Near the ice edge and in the southern part of the bay the ice compactness was 50–80%. The wind forcing data came

from the Finnish Meteorological Institute (FMI) station data (Kemi-1, Marjaniemi and Ulkokalla) and the Swedish Meteorological and Hydrological Institute (SMHI) geostrophic wind data of $1^\circ \times 1^\circ$ grid. The station wind data were adjusted to winds at the standard 10-m anemometer height (Fissel and Tang, 1991). The speed ratio and tuning angle between surface wind and geostrophic wind were 0.6 and 34° based on Bumke *et al.* (1998), respectively. The values are consistent with the studies based on drift buoy observations in the Weddell Sea (Vihma *et al.*, 1996; Uotila *et al.*, 2000). These wind data have 3 hours time interval. They were first spatially interpolated into the ice model grid by a simple objective analysis procedure and then linearly interpolated for 1 hour time intervals. The simulation was performed for 20 days (3–23 March), which covers the whole experiment period. Ice rheology parameters used in the model are $P^* = 3.0 \times 10^4 \text{ Nm}^{-2}$, $e=2.0$, $C=20$ and $\dot{\epsilon}_0 = 10^{-10} \text{ s}^{-1}$ (Hibler, 1979; Zhang *et al.*, 1999).

3.3 Comparison of model results and drifter data

Five drifters were deployed on the drift ice zone by a helicopter during 5–7 March (Haapala and Stipa, 1997). The initial geometry of the drifter locations (see Fig. 4) formed a square with four drifters at each corner (NE-556, NW-557, SE-558 and SW-559) and one at the center (CE-540). The side of the square was about 18 km. The observed and simulated ice drift trajectories for the periods of data being available are shown in Fig. 5.

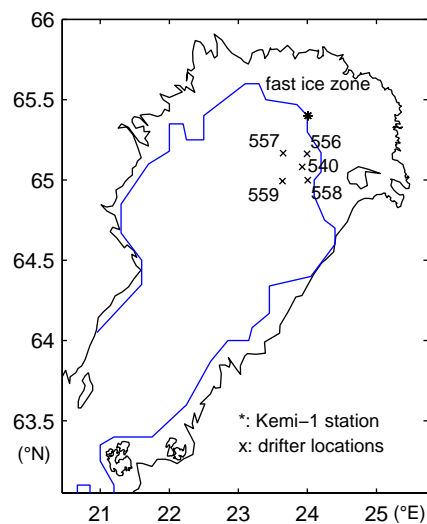


Fig. 4. The initial locations of the GPS drifters.

It can be seen that all drifters traveled first northeastward during the first period. Owing to high compression within the ice pack, the ice cover moved very slowly and the displacements during 5–13 March were only a few kilometers for the eastern drifters (556, 558 and 540) and about 6 and 9 km for the western drifters (557 and 559). The drifter 556 and 540 stopped working on 12 and 13 March, respectively, due to

severe ice conditions. A visual comparison between model results and observed data indicates that the agreement is quite good for all drifters during this period.

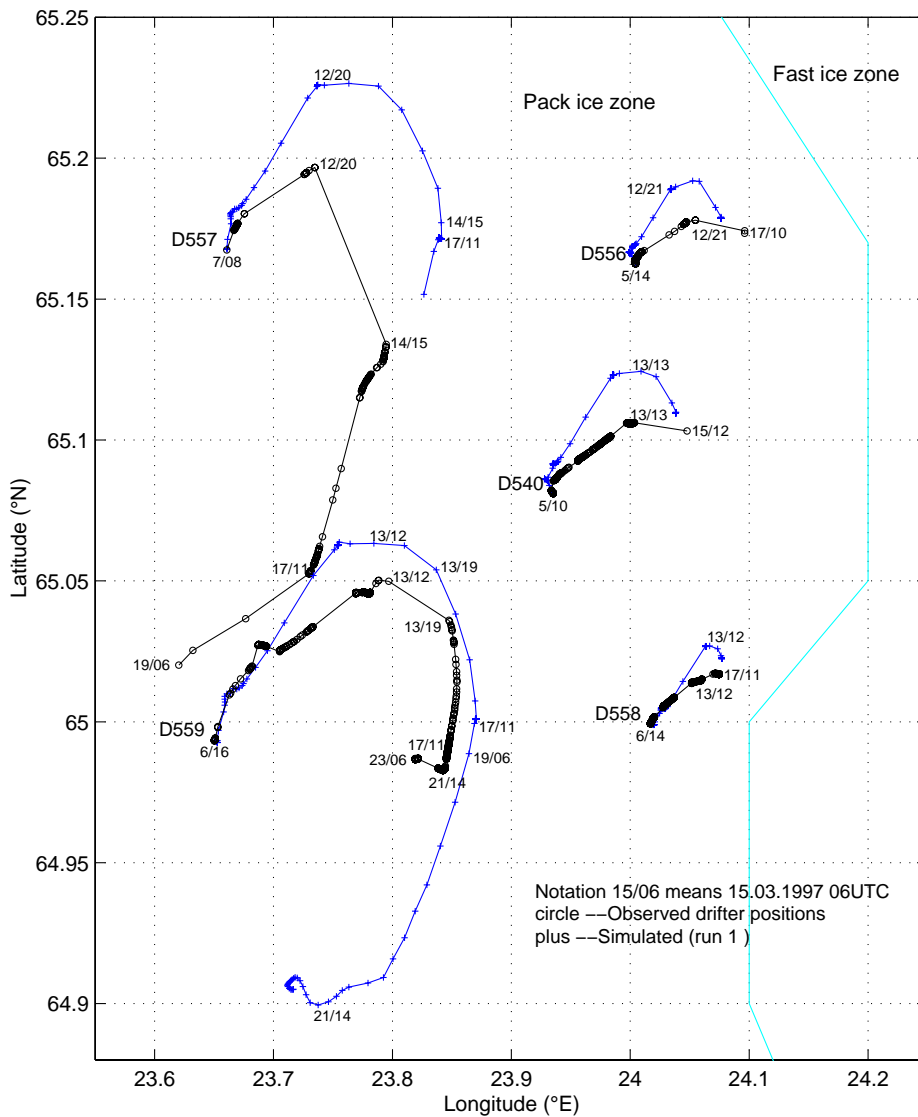


Fig. 5. Observed (circle marks) and simulated (plus marks) GPS drifter trajectories during the experiment period.

In the second period, the wind direction was changed and northerly winds prevailed. The eastern drifters were almost stationary with only small displacements (drifter 556 and 540 were found by helicopter about 2 km eastward away from their last positions on 15 and 17 March, respectively). Drifter 559 also moved slowly with a southward displacement about 7 km. Drifter 557, however, displayed large mobility, which was significantly different from the other four. It traveled about 15 km southwestward during 14–19 March. The model results still show good agreement for drifters 540, 556, 558 and 559 (before 19 March). However, large discrepancies are found for drifter 557 during the period 14–19 March for which the big displacements cannot be reproduced by the model. Large discrepancies are also found at drifter 559 after 19

March for which the model results illustrate larger displacements than the observed data.

A synchronous comparison of ice deformation polygons is shown in Fig. 6. We see that the main discrepancies between model results and observed data are from drifter 557. A possible reason is that there existed strong shear line between drifter 557 and other four during 14–19 March, resulting in large deformation in the real ice field that was not simulated by the model.

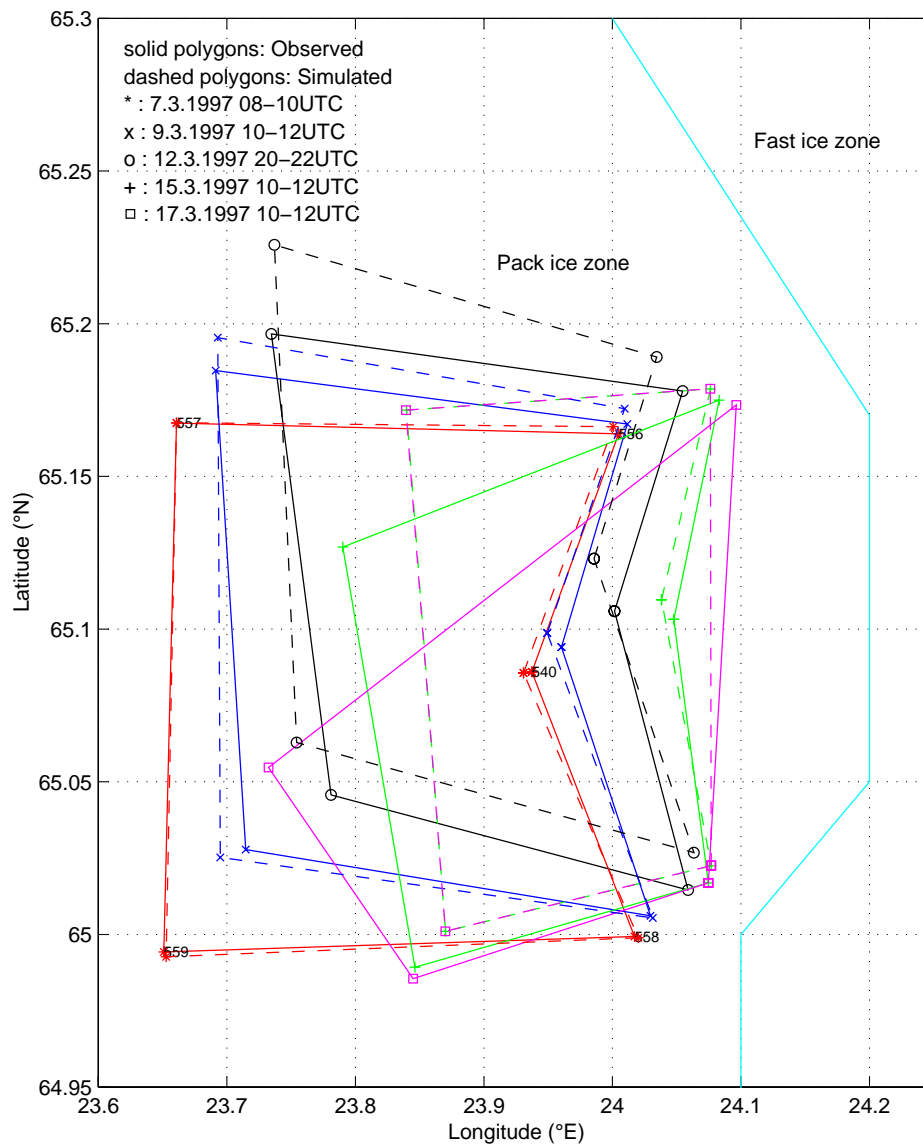


Fig. 6. Observed (solid lines) and simulated (dashed lines) drifter deformation polygons during the experiment period.

Figs. 7–8 show the comparison of the ice kinematics pattern between model calculation and analysis of GPS drifter observations. There were two periods at which polygon deformation area (see Fig. 7) was rapidly changed, indicating large ice field deformations occurred. To quantitatively identify the ice deformation, two-dimensional ice deformation tensor, expressed by two principal ice stresses and vorticity, was cal-

culated and demonstrated in Fig. 8. We see that the order of magnitude of the principal stresses were mostly 10^{-6} s^{-1} , but it could be increased by two order of the magnitude when large deformations occurred. These features are realistically reproduced by the model.

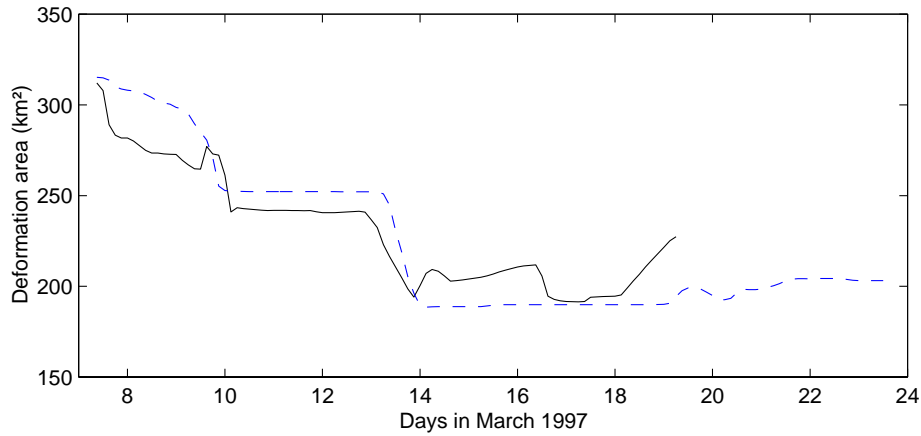


Fig. 7. Observed (solid line) and simulated (dashed line) deformation polygons areas during the experiment period.

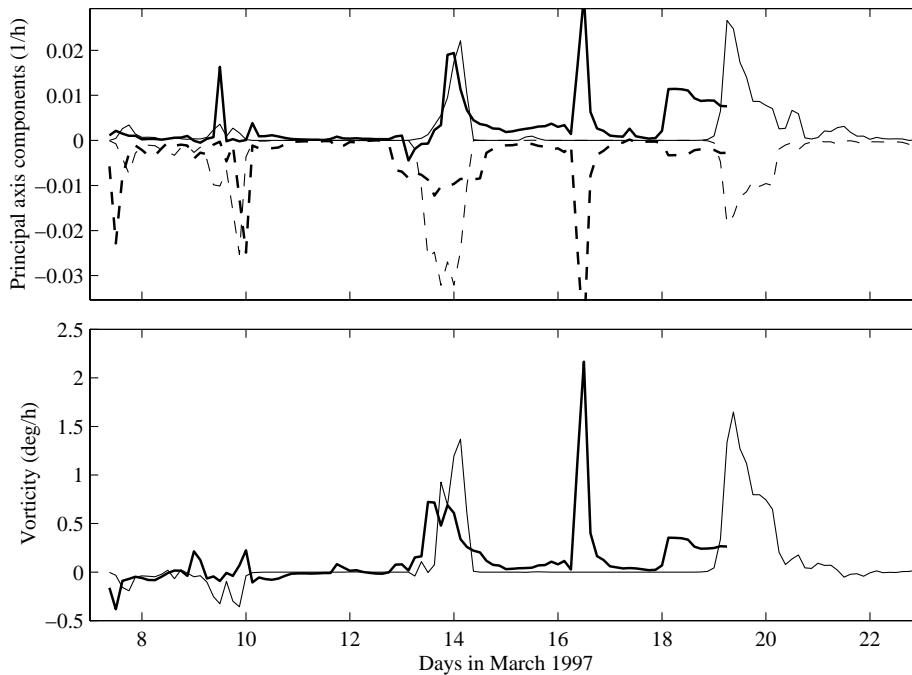


Fig. 8. Observed (bold lines) and simulated (thin lines) principal strain rates (upper panel) as well as vorticity (lower panel). The solid and the dashed lines are the first and second principal components, respectively.

3.4 Comparison of model results and observed data in the basin scale

Comparison with sequential SAR data (Sandven *et al.*, 1997) on the basin wide scale has been also made and is illustrated in Fig. 9. The model results show good

agreement in the coastal ice zone. Note, the displacements from the model are in closer agreement with the drifter data than with the displacements in the SAR data for the period 12–15 March. There are large discrepancies out of the coastal ice zone. The magnitude of model displacements is only about half of the SAR data. Fig. 10 shows the RESURS MSU-SK satellite optical image on 18 March 1997. It is clearly seen that there was a long sharp shear line out of the coastal ice zone, resulting in a discontinuous pattern of the ice drift field on both sides of the shear line (also see Fig. 9) which is hard to simulate. On the other hand, the possible sources of these discrepancies can be produced by several factors related to both the model and the data, for instance, neglect of thermodynamics process of ice and ocean currents, uncertainty of the model parameters and errors from the wind forcing data and the SAR data.

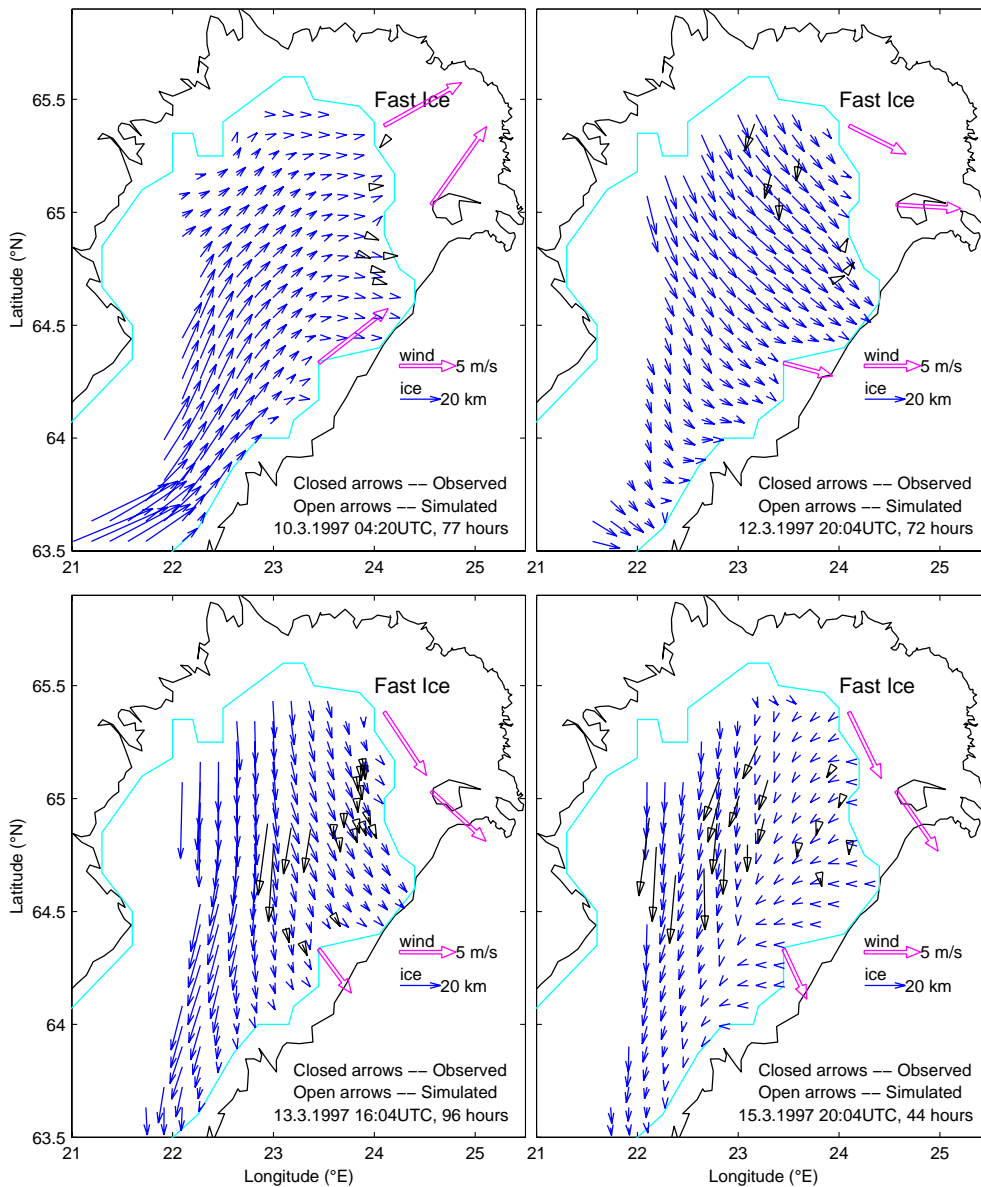


Fig. 9. Comparison of ice displacements between model results and SAR data. The SAR displacement data are obtained from NERSC (*Sandven et al., 1997*).

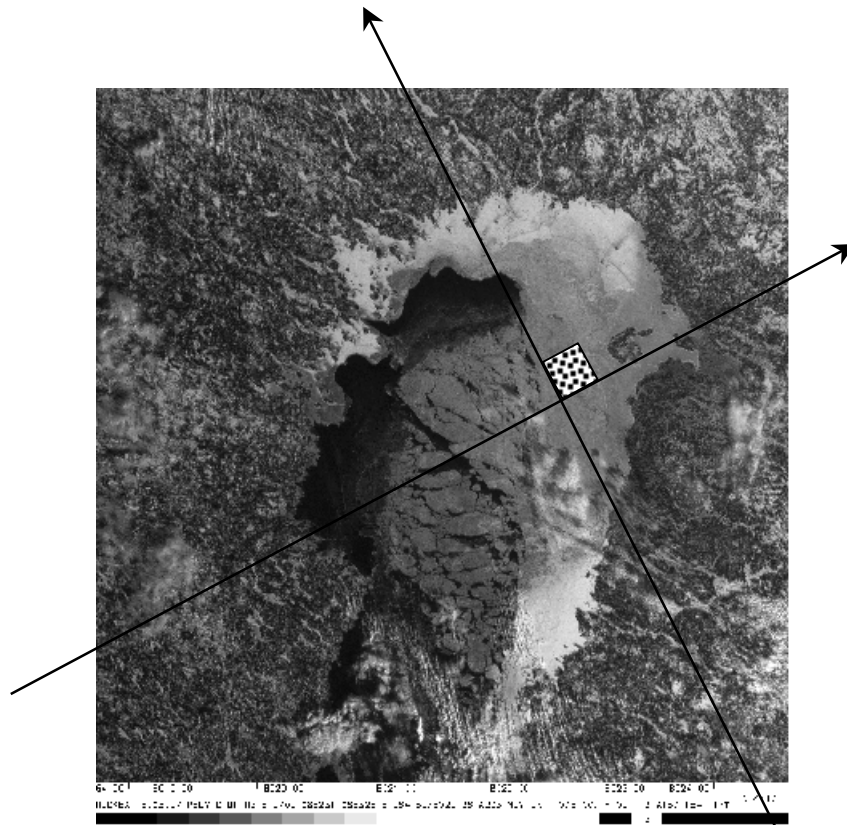


Fig. 10. The RESURS MSU-SK satellite optical image from 18 March 1997. The marked region indicates the initial deployment of the GPS drifters.

The modeled ice thickness fields on March 6, 10, 13 and 20 are illustrated in Fig. 11. Compared with Fig. 3, we see that the thickness redistribution in the real ice fields showed large variability in time and space. The heavy ridge buildup formed along the Finnish coastline and the large opening areas formed in the west and north sides during the experiment period. These can be fairly well reproduced by the model and the overall agreement is good.

The ice strength constant P^* plays an important role in the ice rheology formulation. Some earlier studies (e.g., *Leppäranta and Zhang, 1992; Zhang and Leppäranta, 1995; Leppäranta et al., 1998*) indicated that P^* may vary from $1.0 \times 10^4 \text{ N/m}^2$ to $5.0 \times 10^4 \text{ N/m}^2$ depending on ice conditions in the Baltic Sea. *Leppäranta et al. (1998)* suggested $P^* = 2.5 \times 10^4 \text{ N/m}^2$ being an adequate value for ice modeling using a 10 km model. In the present work the best representation of the ice strength constant suggested $P^* = 3.0 \times 10^4 \text{ N/m}^2$, which is a consistent with *Leppäranta et al. (1998)* but is about three times of *Leppäranta and Zhang (1992)*. Perhaps, the ice field studied here was so close to the solid boundary that the ice showed strong rigid and plastic patterns than in other areas.

Fig. 11. Modeled thickness distributions on March 6, 10, 13, 20 (notated by 72, 168, 240 and 408 hours), 1997, respectively.

4. *Conclusions*

We have developed a high spatial resolution (5 km grid size) dynamic sea ice model capable of applying for coastal seas. The model is based on *Hibler (1979)* viscous-plastic model. A truncated elliptical yield curve that can prevent occurrence of any tensile stress is used. An efficient numerical method for solving momentum balance (*Zhang and Hibler, 1997*) is employed. A simulation for ice drift observations in the Bay of Bothnia was made. The results show that the present model is able to produce a realistic simulation of the observed ice motion and the overall agreement is very encouraging. A visual analysis of the ice floe sizes from the satellite images (*Sandven et al., 1997*) during the experiment period were typically around 300–500 m, which were about ten times less than the model grid size. This indicates that it is possible to reduce model grid size to 5 km for the Baltic Sea without severely violating the continuum ap-

proximation in the Hibler model. The ice field demonstrated strong rigid and plastic features and the value of ice strength constant $P^*=3.0 \times 10^4 \text{ Nm}^{-2}$ is a suitable value for this case. Comparison with SAR displacement data shows that the agreement in the coastal ice zone is good, but there are large discrepancies near the ice edge.

The sources of discrepancies between model results and observed data can be accounted for factors related to both the model and the data. These include incomplete physics of the model, uncertainty of the model parameters and errors of the data. The present model is an isotropic model, which is not able to simulate anisotropic behavior that is often observed in real ice fields. The model parameters (drag coefficients and rheology parameters) used in the model simulation are constant. These values, as illustrated by *Leppäranta et al.* (1998), may be different in time and space in the Baltic Sea. The wind forcing data used in the simulation have an interval of three hours and hence are unable to reproduce ice motion under conditions of rapidly varying wind field. Furthermore, errors in the initial ice fields, lack of an ocean model in providing realistic water currents, and influence of ice thermodynamics may also be causes of the discrepancies.

Although the present model provides satisfactory results of ice drift, further improvements are still needed. An anisotropic model, which could generate open leads, is worthwhile developing and more complex rheology should be considered. Problems such as these require a very careful study of physical basis for relation between stress and strain-rate, which is expected to be possible with the help of more accurate and detailed observations.

Acknowledgements

Author would like to express thanks to Prof. Matti Leppäranta, Dr. Jari Haapala and Tapani Stipa for their help in data analysis and discussions, to Antti Herlevi for providing satellite image. Author would like to thank Dr. Jinlun Zhang for providing model code of the efficient numerical method for solving momentum balance. This work is part of the project Local Cover Deformation and Mesoscale Ice Dynamics or ICE STATE supported by the European Commission, DG XII, through the Marine Science and Technology programme 1994–1998 (MAST III) under contract MAS3–0006. The participants in the joint project are Helsinki University of Technology, Nansen Environment and Remote Sensing Center, Scott Polar Research Institute, University of Helsinki, and University of Iceland.

References

- Bumke, K., U. Karger, L. Hasse and K. Niekamp, 1998. Evaporation over the Baltic Sea as an example of a semi-enclosed sea, *Contr. Atmos. Phys.*, **71**, 249–261.
- Fissel, D.B. and C.L. Tang, 1991. Response of sea ice drift to wind forcing on the Northeastern Newfoundland Shelf, *J. Geophys. Res.*, **96**, 18397–18409.

- Haapala, J. and M. Leppäranta, 1996. Simulations of the ice season in the Baltic Sea, *Tellus*, **48A**, 622–643.
- Haapala, J. and M. Leppäranta, 1997. ZIP-97 Data Report. Haapala and Leppäranta (Eds.), *Report Series in Geophysics*, **37**, University of Helsinki, 122 p.
- Haapala, J. and T. Stipa, 1997. GPS drifters, In: Haapala and Leppäranta (Eds.), *Report Series in Geophysics*, **37**, University of Helsinki, 59–67.
- Hibler III, W.D. 1979. A dynamic and thermodynamic sea ice model, *J. Phys. Oceanogr.*, **9**, 815–846.
- Hibler III, W.D. and E.M. Schulson, 1997. On modeling sea-ice fracture and flow in numerical investigations of climate, *Annals of Glaciology*, **25**, 26–32.
- Hopkins, M.A., 1996. On the mesoscale interaction of lead ice and floes, *J. Geophys. Res.*, **101**, 18315–18326.
- Leppäranta, M. 1981. On the structure and mechanics of pack ice in the Bothnian Bay, *Finnish Mar. Res.*, **248**, 3–86.
- Leppäranta, M. and A. Omstedt, 1990. Dynamic coupling of sea ice and water for an ice field with free boundaries, *Tellus*, **42A**, 482–495.
- Leppäranta, M. and Z.H Zhang, 1992a. A viscous-plastic ice dynamics test model for the Baltic Sea, *Finnish Institute of Marine Research, Internal Rep.* 1992(3), 14 p.
- Leppäranta, M. and Z.H Zhang, 1992b. Use of ERS-1 SAR data in numerical sea ice modeling, In: *Proc. of the Central Symp. of the ISY Conf.*, 30 March-4 April 1992, Munich, Germany (ESA SP-341, July 1992), pp. 123–128.
- Leppäranta, M., Y. Sun and J. Haapala, 1998. Comparisons of sea-ice velocity fields from ERS-1 SAR and a dynamic model, *J. Glaciology*, **147**, 248–261.
- Sandven, S., V. Alexandrov, M. Lundhaug, K. Kloster, T. Hamre and O. Dalen, 1997. Satellite remote sensing of sea ice in the Bothnian Bay during March 1997, *NERSC Technical Report No. 130*, 66 p.
- Uotila, J., T. Vihma and J. Launiainen, 2000. Response of the Weddell Sea pack ice to wind forcing, *J. Geophys. Res.*, **105**, 1135–1151.
- Vihma, T., J. Launiainen and J. Uotila, 1996. Weddell Sea ice drift: Kinematics and wind forcing, *J. Geophys. Res.*, **101**, 18279–18296.
- Wu, H.D. and M. Leppäranta, 1990. Experiments on numerical sea ice forecasting in the Bohai Sea, In: *Proc. IAHR ice Symp.*, Espoo, Finland, 173–186.
- Zhang, J. and W.D. Hibler III, 1997. On an efficient numerical method for modeling sea ice dynamics, *J. Geophys. Res.*, **102**, 8691–8702.
- Zhang, Z.H. and M. Leppäranta, 1995. Modeling the influence of ice on sea level variations in the Baltic Sea, *Geophysica*, **31(2)**, 31–45.
- Zhang, Z.H., M. Leppäranta, J. Haapala and T. Stipa, 1999. Numerical simulation of sea ice drift in the Bay of Bothnia. In: Tuhkuri and Riska (Eds.), *Proc. of the 15th Int. Conf. On Port and Ocean Engin. Under Arctic Conditions*, August 23–27, Espoo, Finland, pp. 488–497.